AIRS Deconvolution and Translation from AIRS to CrIS IR Sounders

**** DRAFT ****

Howard E. Motteler
L. Larrabee Strow

UMBC Atmospheric Spectroscopy Lab
Joint Center for Earth Systems Technology

February 12, 2017

1 Introduction

Upwelling infrared radiation as measured by the AIRS [1], IASI [3], and CrIS [2, 7] sounders is a significant part of the long term climate record. We would like to treat this information as a single data set but the instruments have different spectral resolutions, channel response functions, and band spans. As a significant step in addressing this problem we consider several channel radiance translations—IASI to high resolution CrIS, IASI to AIRS, AIRS to standard resolution CrIS, and high resolution CrIS to AIRS.

Translation from AIRS to CrIS presents a special challenge because CrIS and IASI are Michaelson interferometers with parametrized response functions, while AIRS is a grating spectrometer with channel center frequencies and individually tabulated spectral response functions determined by the focal plane geometery. In section 2 we show how to take advantage of detailed knowledge of the AIRS spectral response functions (SRFs) to deconvolve AIRS channel radiances to a resolution-enhanced intermediate representation.

The translations presented here are validated by comparison with calculated reference truth. For example to test the IASI to AIRS translation we start with 49 fitting profiles spanning a significant range of atmospheric conditions [4, 6]. Upwelling radiance is calculated at a 0.0025 cm^{-1} grid with kcarta [5] over a band spanning the AIRS and IASI response functions. "True AIRS" is calculated from this by convolving the kcarta radiances with AIRS SRFs, and "true IASI" by convolving kcarta radiances to the IASI instrument specifications. IASI is then translated to AIRS (we call this "IASI AIRS") and compared with true AIRS. This sort of validation assumes perfect knowledge of the AIRS and IASI instrument response functions and so gives only a lower bound on residuals, and on how well the translations can work in practice. The better we know the response functions, the closer practical translations can approach these limits.

The conversions here are presented in order of the size of the residuals, with IASI to high resolution CrIS most accurate and high resolution CrIS to AIRS the least. After the sections on translation, the AIRS deconvolution is examined in greater detail. This report is the theoretical basis document for the sounder radiance translations implemented in the airs_decon and iasi_deon git repositories. In addition to the translations, the repositories include the test and validation code used to produce the results shown here. They are available at github,

```
https://github.com/strow/airs_deconv.git
https://github.com/strow/iasi_decon.git
```

2 AIRS Deconvolution

The AIRS spectral response functions model channel response as a function of frequency and associate channels with nominal center frequencies. Each AIRS channel i has an associated spectral response function or SRF $\sigma_i(v)$ such that the channel radiance $c_i = \int \sigma_i(v) r(v)\, dv$, where r is radiance at frequency v. The center or peak of σ_i is the nominal channel frequency.

Figure 1 shows a typical subset of AIRS SRFs. Note the significant overlap in the wings. This allows the deconvolution to recover resolution beyond that of the response functions considered individually. The spacing of the AIRS L1b channels is not regular; there are both gaps and close neighbors, side effects of the focal plane geometry. Both the gaps and close neighbors cause problems for a deconvolution. The AIRS L1c channel set [**?**] is a derived

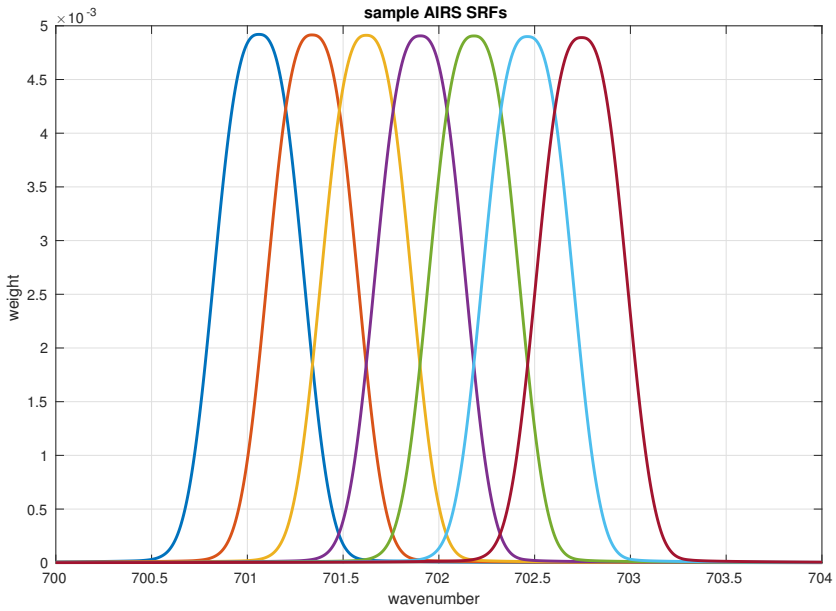

Figure 1: sample adjacent AIRS spectral response functions

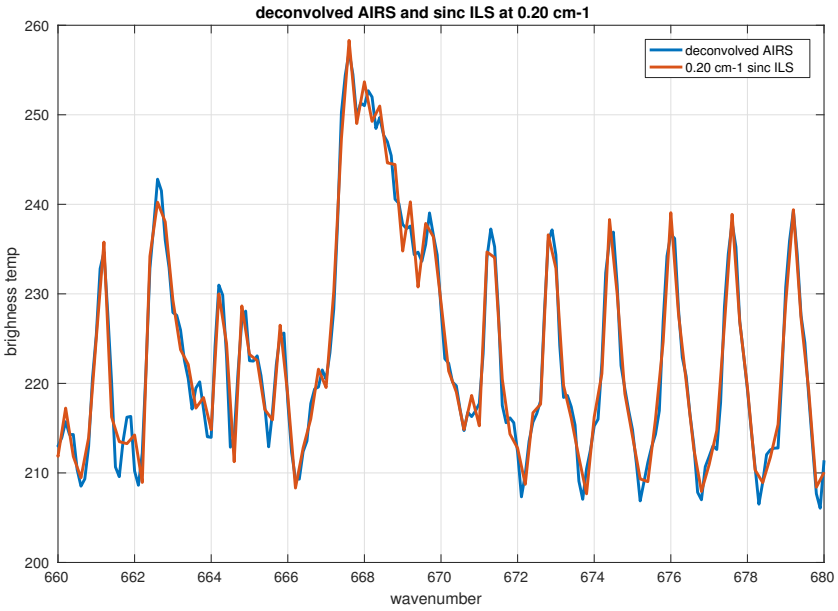

Figure 2: deconvolved AIRS and kcarta 0.0025 cm^{-1} radiances convolved to a sinc ILS at 0.2 cm^{-1}

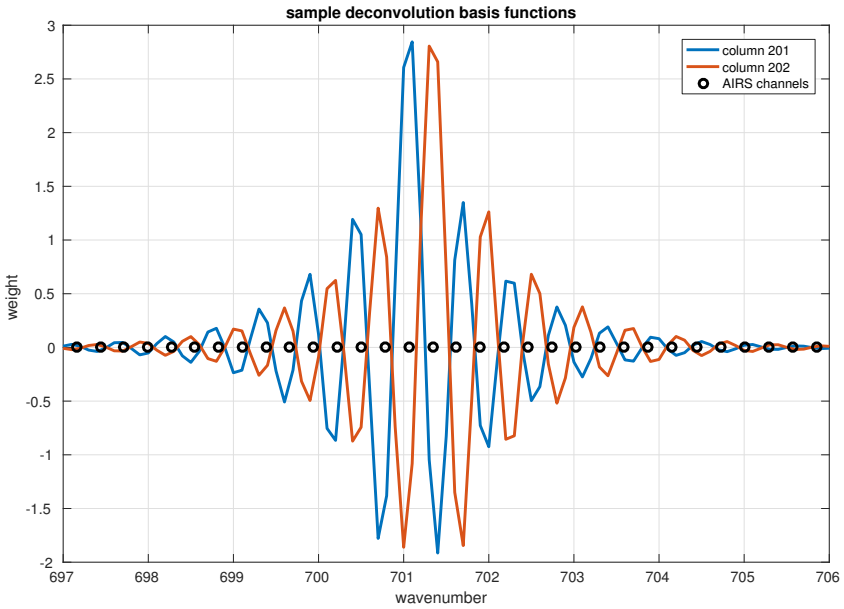

Figure 3: sample basis function for deconvolved AIRS radiances

product of the 1b set with filled gaps and relatively regular (though still frequency dependent) frequency spacing, and we will use the 1c set here.

Suppose we have n channels and a frequency grid $\mathbf{v}$ of k points spanning the domains of the functions σ_i. The grid step size for our applications is often 0.0025 cm^{-1}, the kcarta resolution. Let S_k be an $n \times k$ array such that $s_{i,j} = \sigma_i(v_j)/w_i$, where $w_i = \sum_j \sigma_i(v_j)$, that is where row i is $\sigma_i(v)$ tabulated at the grid $\mathbf{v}$ and normalized so the row sum is 1. If the channel centers are in increasing order S_k is banded, and if they are not too close the rows are linearly independent. S_k is a linear transform whose domain is radiance at the grid $\mathbf{v}$ and whose range is channel radiances. If r is radiance at the grid $\mathbf{v}$, then $c = S_k r$ gives a good approximation of the channel radiances $c_i = \int \sigma_i(v) r(v)\, dv$.

In practice this is how we convolve kcarta or other simulated radiances to get AIRS channel radiances. We construct S_k either explicitly or implicitly from AIRS SRF tabulations. The matrix S_k in the former case is large but manageable with a banded or sparse representation.

Suppose we have S_k and channel radiances c and want to find r, that is, to deconvolve c. Consider the linear system $S_k x = c$. Since $n < k$ for the kcarta grid mentioned above this is underdetermined, with infinitely many

solutions. We could add constraints, take a pseudo-inverse, consider a new matrix S_b with columns tabulated at some coarser grid, or some combination of the above.

For an AIRS to CrIS translation we are mainly interested in the transform S_b with SRFs at an intermediate grid, typically 0.1 cm^{-1}, the approximate resolution of the SRF measurements. Let $\mathbf{v}_b = v_1, v_2, \ldots, v_m$ be a 0.1 cm^{-1} grid spanning the domains of the functions σ_i. Similar to S_k, let S_b be an $n \times m$ array where row i is $\sigma_i(v)$ tabulated at the $\mathbf{v}_b$ grid, with rows normalized to 1. If r is radiance at the $\mathbf{v}_b$ grid, then $c = S_b r$ is still a reasonable approximation of $\int \sigma_i(v) r(v)\, dv$.

Consider the linear system $S_b x = c$, similar to the case $S_k x = c$ above, where we are given S_b and channel signals c and want to find radiances x. Since $n < m < k$, as with S_k the system will be underdetermined but more manageable because m is approximately 40 times less than k. We use a Moore-Penrose pseudoinverse as S_b^{-1}. Then $x = S_b^{-1} c$ gives us deconvolved radiances at the SRF tabulation grid.

The AIRS deconvolution gives a significant resolution enhancement. Figure 2 shows LW detail of deconvolved AIRS together with kcarta radiances convolved directly to a 0.2 cm^{-1} sinc ILS. Figure 3 shows a typical basis function for the AIRS deconvolution, that is, a column of the pseudo-inverse S_b^{-1}.

3 AIRS to CrIS translation

For the CrIS standard resolution mode the channel spacing is 0.625 cm^{-1} for the LW, 1.25 cm^{-1} for the MW, and 2.5 cm^{-1} for the SW bands. The IASI deconvolution was the key step in the IASI to CrIS and IASI to AIRS translations. Similarly, AIRS deconvolution is central to the AIRS to CrIS translation and is presented in detail in section 2. The first step in the AIRS L1c to CrIS translation is to deconvolve the AIRS channel radiances to a 0.1 cm^{-1} intermediate grid, the nominal AIRS SRF resolution. Then for each CrIS band,

- find the AIRS and CrIS band intersection
- apply a bandpass filter to the deconvolved AIRS radiances to restrict them to the intersection, with a rolloff outside the intersection

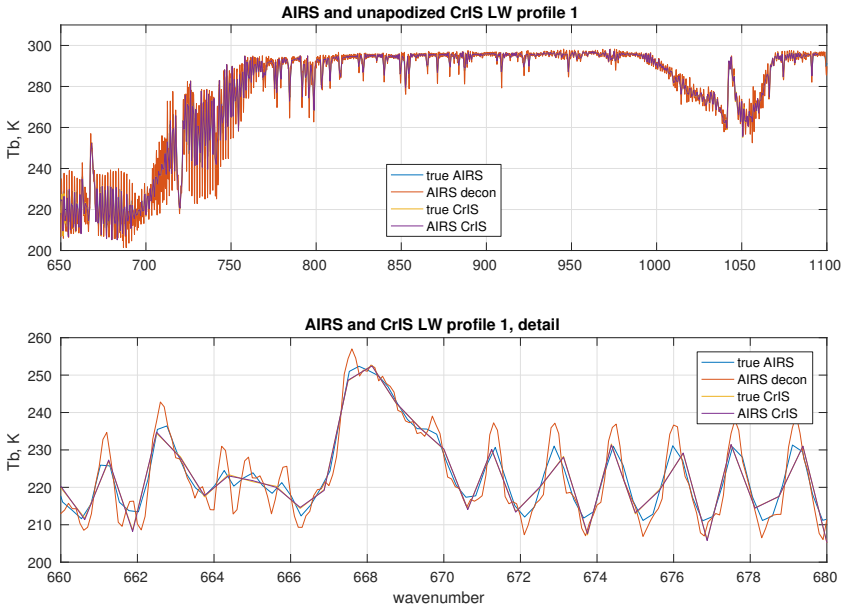

Figure 4: true CrIS, true AIRS, deconvolved AIRS, and AIRS CrIS

- reconvolve the filtered spectra to the CrIS user grid

Figure 4 shows true CrIS, true AIRS, deconvolved AIRS, and AIRS CrIS. At this level of detail we mainly see the greater fine structure in the deconvolution. Figure **??** shows details from 660 to 680 cm^{-1}. Note the similarity to the IASI deconvolution in figure **??**. The remaining figures show true CrIS minus AIRS CrIS for the 49 fitting profiles, with and without Hamming apodization for each of the CrIS bands. The residuals are significantly reduced with apodization but are larger than for the IASI to CrIS translation.

For the AIRS to CrIS translation deconvolution works better than both simple interpolation and interpolation (rather than deconvolution) to an intermediate grid followed by convolution to CrIS radiances. For the first case we start with true AIRS and interpolate radiances directly to the CrIS user grid with a cubic spline. For the second we interpolate true AIRS to the 0.1 cm^{-1} intermediate grid with a cubic spline and then convolve this to the use CrIS user grid.

Figure 11 shows interpolated CrIS minus true CrIS for both interpolation tests for the LW band, without any apodization. While the two-step interpolation works a little better than the simple spline, both residuals are

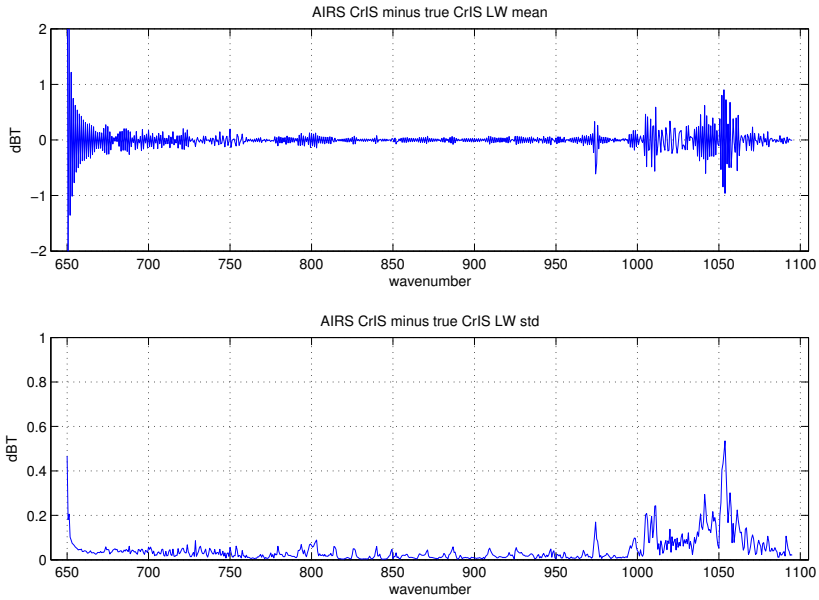

Figure 5: Mean and standard deviation of unapodized AIRS CrIS minus true CrIS, for the CrIS LW band

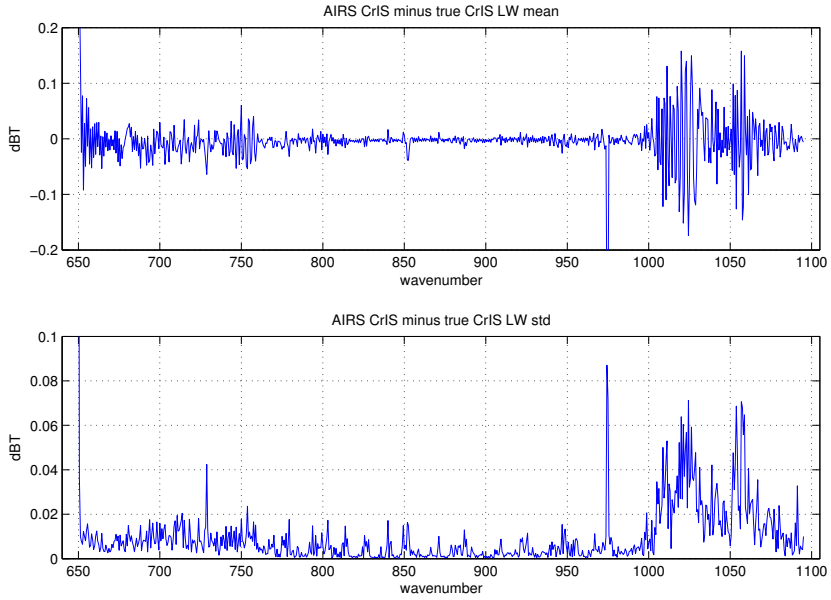

Figure 6: Mean and standard deviation of Hamming apodized AIRS CrIS minus true CrIS, for the CrIS LW band

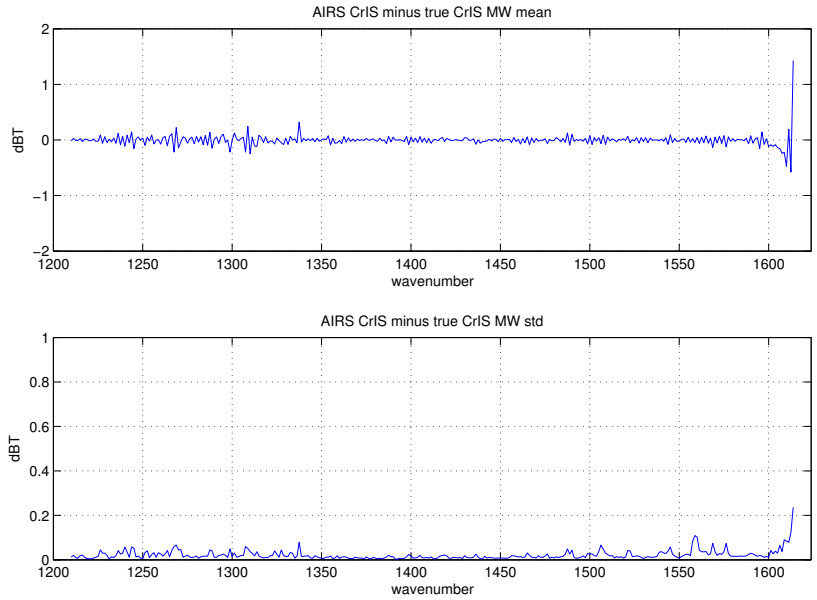

Figure 7: Mean and standard deviation of unapodized AIRS CrIS minus true CrIS, for the CrIS MW band

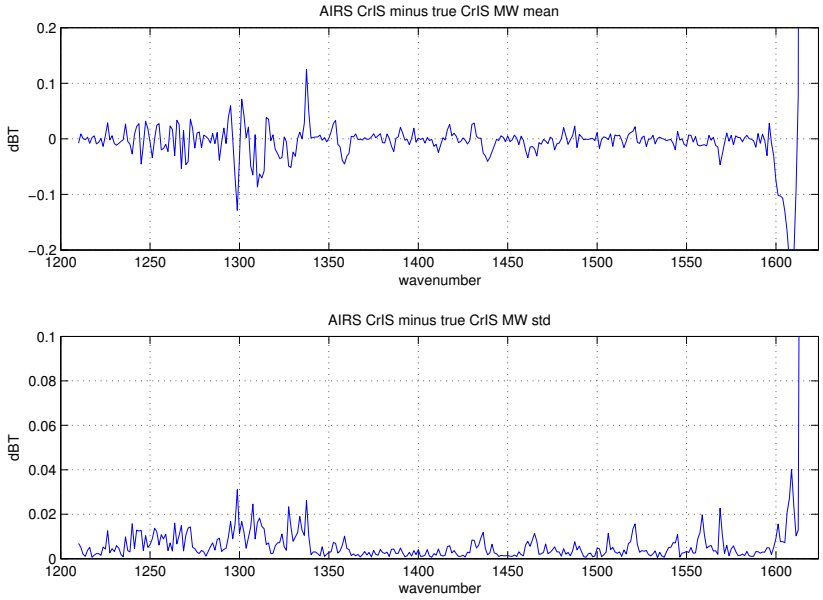

Figure 8: Mean and standard deviation of Hamming apodized AIRS CrIS minus true CrIS, for the CrIS MW band

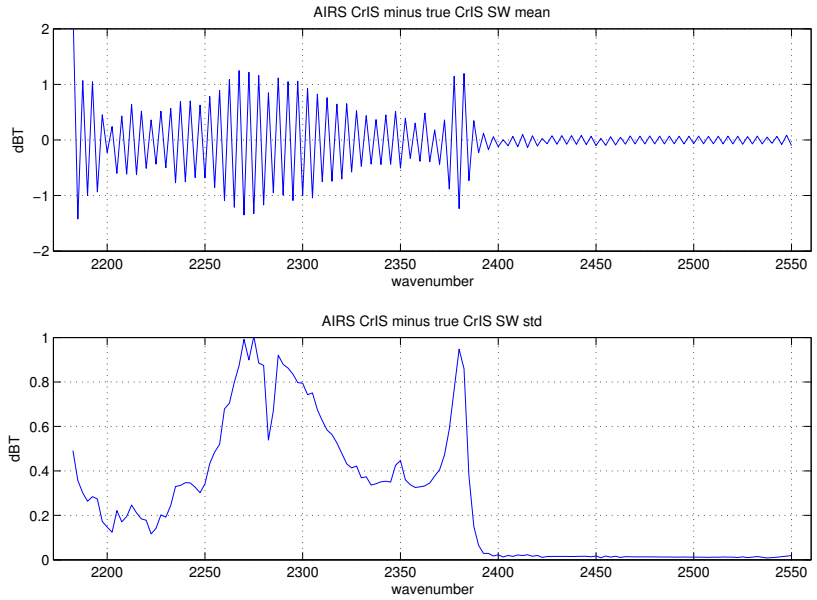

Figure 9: Mean and standard deviation of unapodized AIRS CrIS minus true CrIS, for the CrIS SW band

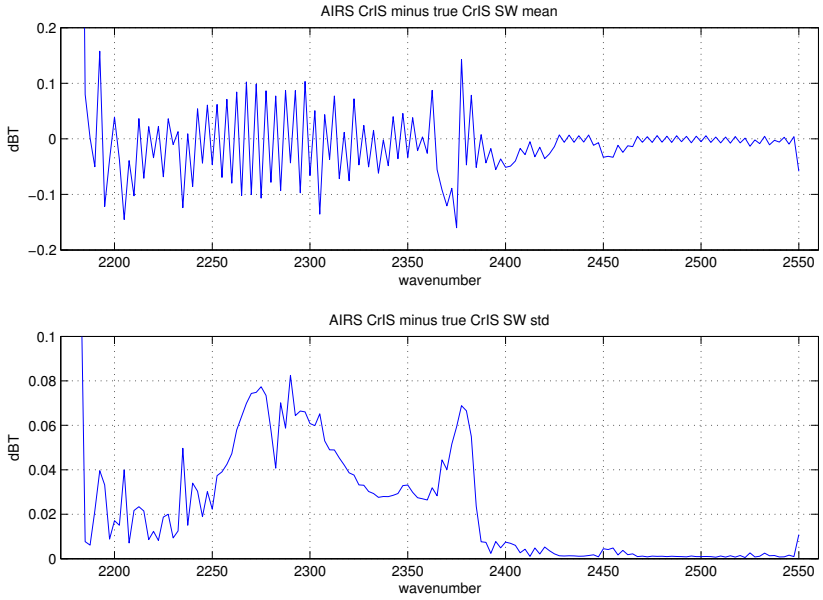

Figure 10: Mean and standard deviation of Hamming apodized AIRS CrIS minus true CrIS, for the CrIS SW band

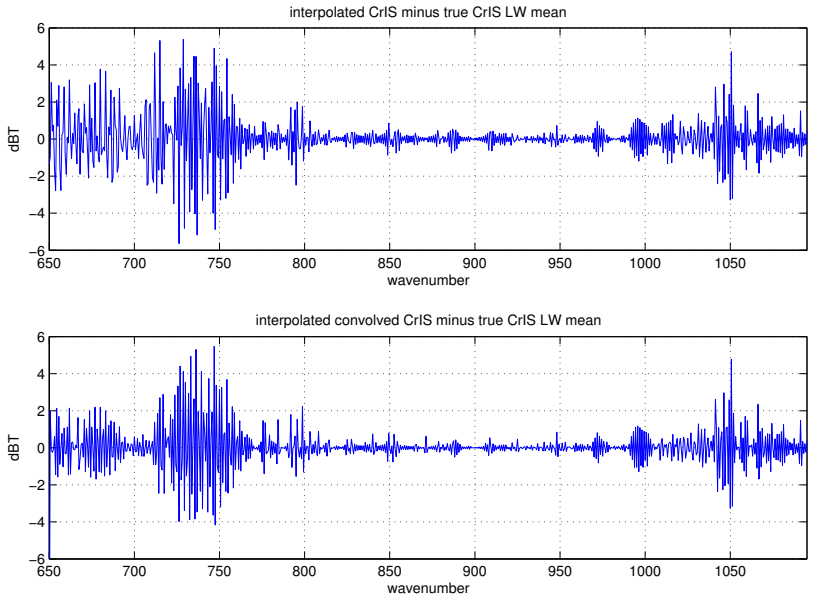

Figure 11: simple interpolation and interpolation with convolution, for the CrIS LW band

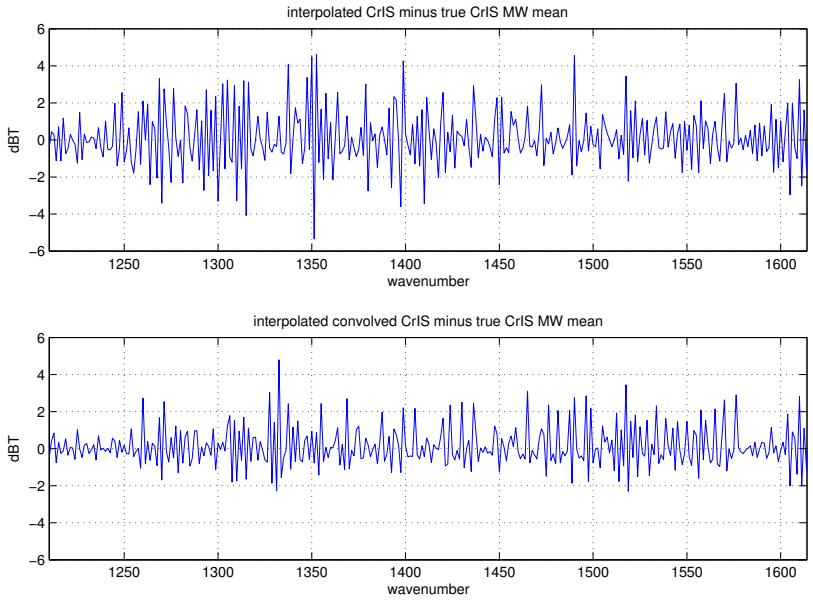

Figure 12: simple interpolation and interpolation with convolution, for the CrIS MW band

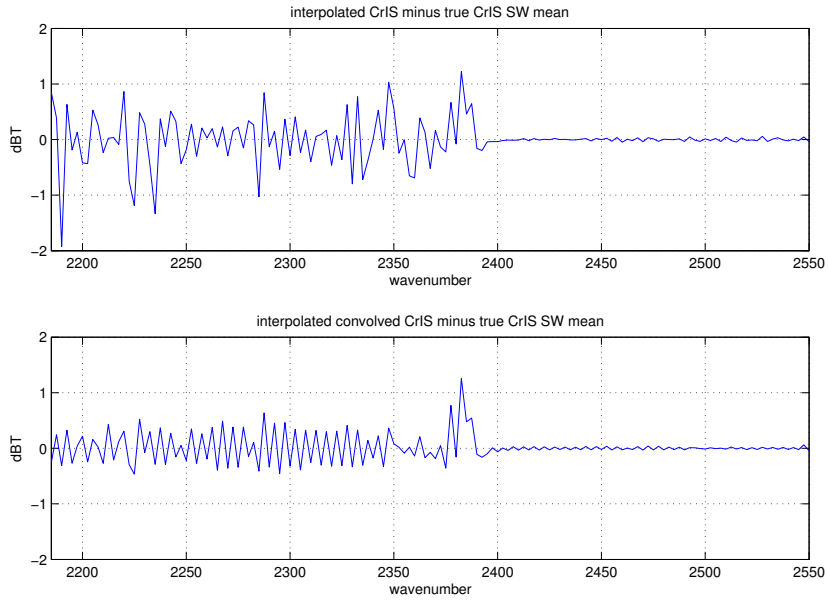

Figure 13: simple interpolation and interpolation with convolution, for the CrIS SW band

significantly larger than for the translation with deconvolution shown in figure 5. Figures 12 and 13 show similar results for the MW and SW bands. Deconvolution is significantly better for the MW, (figure 7) while the comparison is less clear for the SW (figure 9). Comparisons with Hamming apodization show the residuals with deconvolution are significantly less for all three bands.

References

[1] H. H. Aumann, M. T. Chahine, C. Gautier, M. D. Goldberg, E. Kalnay, L. M. McMillin, H. Revercomb, P. W. Rosenkranz, W. L. Smith, D. H. Staelin, L. L. Strow, and J. Susskind. AIRS/AMSU/HSB on the aqua mission: design, science objectives, data products, and processing systems. *IEEE Transactions on Geoscience and Remote Sensing*, 41:253–264, Feb. 2003.

[2] Y. Han, H. Revercomb, M. Cromp, D. Gu, D. Johnson, D. Mooney, D. Scott, L. Strow, G. Bingham, L. Borg, Y. Chen, D. DeSlover, M. Es-

plin, D. Hagan, X. Jin, R. Knuteson, H. Motteler, J. Predina, L. Suwinski, J. Taylor, D. Tobin, D. Tremblay, C. Wang, L. Wang, L. Wang, and V. Zavyalov. Suomi NPP CrIS measurements, sensor data record algorithm, calibration and validation activities, and record data quality. *Journal of Geophysical Research (Atmospheres)*, 118:12734, Nov. 2013.

[3] F. Hilton, R. Armante, T. August, C. Barnet, A. Bouchard, C. Camy-Peyret, V. Capelle, L. Clarisse, C. Clerbaux, P.-F. Coheur, A. Collard, C. Crevoisier, G. Dufour, D. Edwards, F. Faijan, N. Fourrié, A. Gambacorta, M. Goldberg, V. Guidard, D. Hurtmans, S. Illingworth, N. Jacquinet-Husson, T. Kerzenmacher, D. Klaes, L. Lavanant, G. Masiello, M. Matricardi, A. McNally, S. Newman, E. Pavelin, S. Payan, E. Péquignot, S. Peyridieu, T. Phulpin, J. Remedios, P. Schlüssel, C. Serio, L. Strow, C. Stubenrauch, J. Taylor, D. Tobin, W. Wolf, and D. Zhou. Hyperspectral Earth Observation from IASI: Five Years of Accomplishments. *Bulletin of the American Meteorological Society*, 93:347–370, Mar. 2012.

[4] L. Strow, S. Hannon, S. De Souza-Machado, H. Motteler, and D. Tobin. An overview of the airs radiative transfer model. *Geoscience and Remote Sensing, IEEE Transactions on*, 41(2):303–313, Feb 2003.

[5] L. Strow, H. E. Motteler, R. G. Benson, S. E. Hannon, and S. D. Souza-Machado. Fast computation of monochromatic infrared atmospheric transmittances using compressed look-up tables. *Journal of Quantitative Spectroscopy and Radiative Transfer*, 59(35):481 – 493, 1998. Atmospheric Spectroscopy Applications 96.

[6] L. L. Strow, S. E. Hannon, S. De-Souza Machado, H. E. Motteler, and D. C. Tobin. Validation of the atmospheric infrared sounder radiative transfer algorithm. *Journal of Geophysical Research: Atmospheres*, 111(D9), 2006. D09S06.

[7] L. L. Strow, H. Motteler, D. Tobin, H. Revercomb, S. Hannon, H. Buijs, J. Predina, L. Suwinski, and R. Glumb. Spectral calibration and validation of the Cross-track Infrared Sounder on the Suomi NPP satellite. *Journal of Geophysical Research (Atmospheres)*, 118:12486, Nov. 2013.